Catalysis Science & Technology

Accepted Manuscript

ROYAL SOCIETY OF CHEMISTRY

www.rsc.org/catalysis

ARTICLE

Synthetic natural gas by direct CO_2 hydrogenation on activated takovites: Effect of Ni/Al molar ratio

S. Abelló,[a,†] C. Berrueco,[a] F. Gispert-Guirado,[b] and D. Montané[a,c]

Takovite-derived mixed oxides with Ni/Al molar ratios from 1 to 3 have been used as catalysts in CO_2 hydrogenation to CH_4. Catalysts were characterized by XRD, BET, TEM, TGA, H_2-TPR, and monitorized by in situ DRIFTS under reaction conditions. The catalytic performance for the CO_2 methanation has been investigated in a fixed-bed reactor at a temperature range from 225 to 400°C and pressures of 10.0 and 1.0 bar(g). Takovite decomposition leads to the formation of a NiO phase containing Al ions, and a nickel-containing alumina phase (Ni-deficient spinel). The percentage of spinel increases upon decreasing the Ni/Al ratio, and consequently, a lower amount of metallic nickel after subsequent reduction is achieved. All catalysts were partially reduced upon time on stream, leading to the formation of small Ni^0 crystallites (ca. 3 nm) dispersed on a $NiAl_2O_4$ matrix. The most active and selective catalyst was the one with a Ni/Al ratio of 2, which was also very stable after a 500 h lifetime test at atmospheric pressure and 275°C.

Introduction

Global natural gas consumption is increasing at a rate of 1.7 percent per year, being the fuel of choice for electric power and industrial sectors in many regions of the world. In fact, these two sectors account for a 77 percent of the total projected world increase in natural gas consumption. This is in part due to its lower carbon intensity (weight of carbon emitted per unit of energy consumed) compared with oil and coal, which makes it an attractive fuel source in those countries where policies to reduce greenhouse gas emissions are implemented.[1] The production of synthetic natural gas (SNG) from carbon sources (coal, biomass or municipal solid wastes) has attracted an increasing attention as an efficient and clean energy carrier,[2,3] since it benefits from the existing infrastructure for transport and storage of natural gas. The necessity to reduce the dependency from natural gas imports in several regions, and the growing interest in the use of CO_2 as feedstock have motivated the revival of the well-known methanation reaction ($CO_2 + 4\ H_2 \leftrightarrows CH_4 + 2H_2O$).[4] Generally, SNG can be produced by gasification of coal and biomass towards syngas (CO + H_2), which is subsequently transformed into CH_4, and by hydrogenation of captured CO_2.[3,5-8]

The methanation reaction, considering both the hydrogenation of CO and CO_2, has been the subject of a large number of studies in the last century.[9] Many metal-supported methanation catalysts have been developed, and the work by Mills and Steffgen correlated their activity following the order Ru>Ir>Rh>Ni>Co>Os>Pt>Fe>Mo>Pd>Ag.[10] Among these metals, supported Ni-based catalysts are still the choice for the production of SNG due to its relatively high catalytic activity, high CH_4 selectivity, and affordable price.[11-17] Various supports including SiO_2, Al_2O_3, ZrO_2, TiO_2 or CeO_2 have been selected for most investigations.[9,11,12,14-21] Unfortunately, nickel-based catalysts exhibit unsatisfactory deactivation by carbon deposition and nickel sintering at high temperature.

Ni/Al_2O_3 catalyst, either alone or with addition of promoters, is one of the most investigated systems for methanation reactions.[3,14,22-28] Impregnation of Al_2O_3 or eventually, coprecipitation, are the most extended preparation methods for Ni-based methanation catalysts, with nickel loadings from 10 to 125 wt.%.[22,24,27] Promoters like Ce, Mo, or Fe give rise to a wide spectrum of CO_2 conversions (from 5 to 99%) attending to the different experimental conditions (temperature, pressure, space velocity, H_2/CO_2 ratio, and nickel content). Hwang et al.[29] prepared Ni-Fe/Al_2O_3 catalysts with >30% of Ni, reaching relatively small nickel crystallites. CO_2 conversion around 61% and CH_4 selectivity of 99.5% were achieved at low temperature and relatively slow space velocity. No clear relationship was established between the activity and the size of Ni crystallites. Recently, Rahmani et al.[26] found that increasing the Ni loading from 10 to 20 wt.% in Ni/Al_2O_3 catalyst led to increased activity in the reaction, but higher metal loadings induced lower CO_2 conversion. This was attributed to the presence of larger Ni crystallites and lower surface areas. Other authors claimed that pre-reduction of Ni is needed when the Ni loading is below the amount of metal required to cover the alumina surface in Ni/Al_2O_3 catalysts.[27] The same authors concluded that smaller Ni particles avoid CO formation during methanation.

In our previous work,[30] we were guided by the significant influence of the support, Ni loading and metal crystallite size on the dispersion of nickel particles, and therefore, on their performance in methanation. For that, an unpromoted Ni-Al catalyst prepared by coprecipitation with ca. 70 wt.% of Ni, was found very active (83.5 % CO_2 conversion) and selective (>99% to CH_4) after a ca. 500 h lifetime test, using a WHSV one order of magnitude higher than the space velocity reported by other authors at similar temperatures and pressures.[30] Despite the high Ni loading, the preparation method (coprecipitation)

a. *Catalonia Institute for Energy Research (IREC), C/ Marcel·lí Domingo 2, Building N5, Universitat Rovira i Virgili, 43007, Tarragona, Spain.*
b. *Servei de Recursos Científics i Tècnics, Universitat Rovira i Virgili, Avda. Països Catalans 26, 43007, Tarragona, Spain.*
c. *Departament d'Enginyeria Química, Universitat Rovira i Virgili, Avda. Països Catalans 26, 43007, Tarragona, Spain.*
† Corresponding author Fax: +34 977 297 922. e-mail: sabello@irec.cat.
Electronic Supplementary Information (ESI) available: [details of any supplementary information available should be included here]. See DOI: 10.1039/x0xx00000x

and the activation procedure (partial reduction of the oxide) induced the formation of well-integrated small Ni^0 crystallites of ca. 6 nm dispersed over a NiO-alumina matrix, which were active and selective for CO_2 methanation. The coprecipitation route was also investigated by He et al.[31] to prepare a Ni-Al hydrotalcite (3:1) and used in the reaction after direct reduction of the precursor, thus leading to high CO_2 performance. The authors attributed the high activity of this catalyst to the presence of strong basic sites beneficial for CO_2 activation coupled to the presence of small Ni particles (4 nm). Other authors previously found that both Ni/Al ratio and reduction temperature are important parameters to improve the methanation performance over takovite-derived catalysts; that is, a Ni/Al = 3 and reduced at 450°C was found to be optimal.[32]

Based on the markedly distinctive performance of such catalysts, Ni-Al mixed oxides derived from takovite have been prepared with Ni/Al molar ratios from 1 to 3, and investigated in CO_2 methanation. The effect of the Ni/Al molar ratio on the performance of the activated catalysts was studied with the objective to derive structure-performance relationships associated with the nickel loading and dispersion. Activity measurements have been complemented with detailed characterization of the fresh and used solids, and in situ infrared methanation measurements.

Experimental section

Catalyst preparation

Takovites (Ni-Al hydrotalcites) with nominal Ni/Al molar ratio of 3, 2, and 1 were prepared by coprecipitation at constant pH. Aqueous solutions of the metal nitrates (1 M of $Ni(NO_3)_2 \cdot 6H_2O$ and 1 M of $Al(NO_3)_3 \cdot 9H_2O$) and the precipitating agent ($NaOH/Na_2CO_3$, 1 M of each) were simultaneously fed into a polypropylene vessel by a 905 Titrando® automated titrator (Metrohm AG) equipped with two 800 Dosino® dosing systems. The pH during precipitation in the stirred reactor vessel was maintained at a constant value of 9 (±0.1). After addition of the reactants, the product slurry was aged at 30°C for 15 h under stirring. The precipitates thus obtained were filtered and washed with deionized water, and dried overnight at 80°C, to yield the as-prepared takovites (Ni_3Al-P, Ni_2Al-P, and Ni_1Al-P). The three samples were calcined in static air at 450°C for 6 h using a ramp rate of 5°C/min. Prior to characterization studies, the calcined samples were heated in N_2 at 5°C/min to 500°C and reduced at this temperature in a mixture of 10 vol% H_2 in N_2 for 3 h. Afterwards, the reduced samples were stored in N_2 before characterization. Calcined, reduced and used samples recovered after reactions are identified by the codes C, R, and U.

Catalyst characterization

The chemical composition of the solids was determined by inductively coupled plasma-optical emission spectroscopy (ICP-OES) in a Spectro Arcos 165 spectrophotometer. Before analysis, the solids were dissolved in 1 wt.% HNO_3 aqueous solution. Powder X-ray diffraction patterns were acquired in a Siemens D5000 diffractometer (Bragg-Brentano parafocusing geometry and vertical goniometer) fitted with a curved graphite diffracted-beam monochromator, incident and diffracted-beam Soller slits, aperture/divergence slit angle 0.5, scattered-radiation slit angle 0.5, a 0.06 mm receiving slit and scintillation counter as detector. The angular 2θ diffraction range was between 5.0 and 70.0°. The data were collected with an angular step of 0.05° at 3 s per step. Cu_k radiation was obtained from a copper X-ray tube operated at 40 kV and 30 mA. The quantitative phase content of the catalysts was determined by a multiphase Rietveld method[33,34] and using TOPAS software.[35] The crystallite size was estimated by using the Double-Voigt Approach[36] and the Scherrer equation.[37] The contribution of the instrument to the experimental peak width was corrected with a previous analysis on LaB_6 standard (NIST, SRM 660a). It should be noted that this type of analysis is subject to errors due to an oversimplification of the present case for crystallite size determination with the following assumptions: spherical crystallite shape, negligible lattice strain contribution to the reflection width and unimodal particle distribution. N_2 adsorption data were measured on a Quantachrome Quadrasorb-SI gas-adsorption analyzer. Prior to the measurements, the samples were degassed under vacuum at 120°C (as-synthesized) and 300°C (calcined, reduced and used) for 10 h, respectively. Transmission electron microscopy (TEM) was carried out in a JEOL JEM-1011 microscope operated at 100 kV. A few droplets of the sample suspended in ethanol were placed on a carbon-coated copper grid followed by evaporation at ambient conditions. Thermogravimetric analysis (TGA) was measured in a Mettler Toledo TGA/DSC 1 microbalance. Analyses were performed in air (20 NmL/min) ramping the temperature from room temperature to 1000°C at 5°C/min. Temperature-programmed reduction with hydrogen (H_2-TPR) was measured in a ChemBet Pulsar TPR/TPD unit equipped with a thermal conductivity detector. Ca. 50 mg of the oxides obtained by calcination of the takovite precursors at 450°C were loaded in the U-quartz microreactor, pretreated in air (20 NmL/min) at 300°C for 1 h, and cooled to 50°C in the same atmosphere. The analysis was carried out in a mixture of 5 vol% H_2 in N_2 (20 NmL/min), ramping the temperature from 50 to 900°C at 10°C/min. Hydrogen chemisorption was performed on a Quantachrome Autosorb-iQ-C sorption analyzer. The calcined sample (ca. 40 mg) was treated in He at 500°C using a ramp of 5°C/min, and reduced at the same temperature in pure H_2 for the same proportional time than that used before reaction. Afterwards, the sample was evacuated at 500°C for 30 min and cooled to room temperature with an additional evacuation of 5 min. A first H_2 adsorption isotherm was taken at 40°C, which provided the sum of the reversibly and irreversibly adsorbed hydrogen. Then, the sample was evacuated at the same temperature and a second H_2 isotherm was measured, which represented only the reversibly adsorbed hydrogen. The difference between the two isotherms corresponds to the amount of chemisorbed hydrogen on the samples at 40°C. The gas uptake was obtained by extrapolating to zero pressure the linear portion

of the isotherm above saturation pressure. The metal surface area (S_{Ni} in m^2/g), and Ni dispersion (D, in %) were determined from the H_2 chemisorption data, assuming the adsorption stoichiometry of one hydrogen atom per nickel atom (H/Ni = 1) and a Ni surface area of $0.065 \ nm^2/atom$.

Infrared measurements

In this study, the infrared measurements were obtained in a Fourier Transform Infrared Spectrometer (Bruker, Vertex 70) using a DRIFTS reaction cell (Harrick, HVC) with ZnSe windows, and a MCT detector. The reaction cell includes a heating element and a thermocouple, providing the feedback to a temperature controller. Gases were dosed into the cell by mass flow controllers keeping the total flow at 15 NmL/min. The sample holder was filled with powdered Ni catalyst (~10 mg). A dilution ratio of KBr:catalyst of 4:1 was used, and leveled off to reduce reflections off the sample surface. The catalyst was first reduced at 450°C for 1 h in 20 NmL/min of N_2:H_2 (25/75), and subsequently cooled down by steps to 150°C while recording different background spectra. The reduced catalyst was exposed to the mixture containing CO_2/N_2 (16.6/83.4) for CO_2 adsorption studies, and $H_2/CO_2/N_2$ (66.6/16.6/16.6) for methanation studies for an initial period of 30 min at 150°C, and subsequently, temperature was increased at intervals of 50°C to 400°C. Difference spectra related to adsorbed species were obtained by subtracting those corresponding to the reduced fresh catalyst to those obtained under reaction conditions at the same temperature. Spectra were systematically recorded every 120 s in the range 600-4000 cm^{-1} by co-addition of 64 scans at a nominal resolution of 4 cm^{-1}.

Activity tests

The activity and selectivity of the catalyst were tested in a fully automated laboratory scale fixed-bed catalytic reactor (Microactivity Reference, PID Eng&Tech, Spain). Experiments were conducted using ca. 100 mg of catalyst particles sieved to 100-300 μm, which were mixed with ca. 3 g of quartz chips sieved to the same particle sizes. The catalyst was loaded into the reactor tube and heated at 10°C/min to 500°C under N_2 (90 NmL/min), and was then reduced *in situ* for 3 h at this temperature by adding 10 NmL/min of H_2 (10% H_2 concentration). After reduction, the flow rates of H_2, CO_2 and N_2 were adjusted and the reaction test started; N_2 was used as internal standard for the chromatographic analysis of the reaction products. Experiments were conducted using a H_2/CO_2 molar ratio of 4.0, a constant N_2/CO_2 ratio of 1.0, a pressure of 10.0 bar(g), and a space velocity (WHSV) of $0.6 \ mol_{CO2}/(g_{cat}·h)$. Catalyst screening was developed isothermally at intervals of 25°C in the range 400 − 225°C; the tests were run starting at the highest temperature, with a holding time of 5 h at each temperature, and decreasing to the following value at 10°C/min. At the end of the series, temperature was raised again to 400°C at 10°C/min in order to check for deactivation. A test with variation in pressure (10 and 1 bar(g)) was performed over the best catalyst in the same

temperature range. Two lifetime tests were also conducted at atmospheric pressure and a WHSV of $0.8 \ mol_{CO2}/(g_{cat}·h)$, with H_2/CO_2 and N_2/CO_2 molar ratios of 4.00 and 1.00, respectively, at 275 and 350°C. The product gas was cooled to 5°C and the condensed water removed and measured in a scale connected to the unit control system. The composition of the dry gas was determined with an on-line gas micro-chromatograph (490 microGC, Agilent Technologies). Gas samples were automatically analyzed every 3.7 min along the screening experiments. Carbon dioxide conversion (X_{CO2}) and selectivity to the different products (S_j) were calculated according to equations 1 and 2, where F_{CO2_0} is the feed molar flow rate of CO_2, F_j is the molar flow rate of product j at the reactor outlet, and nC_j is the number of carbon atoms in compound j.

$$X_{CO_2} = 100 \cdot \left(\frac{F_{CO_2\_0} - F_{CO_2}}{F_{CO_2\_0}} \right) \tag{1}$$

$$S_j = \left(\frac{nC_j \cdot F_j}{F_{CO_2\_0} - F_{CO_2}} \right) \tag{2}$$

Results and discussion

Precursors

The molar Ni/Al ratio in the solids determined by ICP-OES was close to the nominal ratios (Table 1). Fig. 1 shows the XRD patterns of the as-synthesized materials and the products of calcination, reduction, and after use in the methanation reaction. The parent samples (P) revealed the characteristic reflections of the takovite-type structure $Ni_{0.75}Al_{0.25}(OH)_2(CO_3)_{0.125} \cdot 0.5H_2O$,[38] independently of the Ni/Al ratio. Takovite is a member of the hydrotalcite family (also known as layered double hydroxide, LDH). Broader and less intense reflections were achieved with the lower Ni/Al ratio, indicating the lower crystallinity at lower nickel content. No other reflections associated with single metal hydroxides were visible in any of the samples. From the two typical non-basal (110) and (113) planes at higher 2θ, only the first reflection was clearly discerned at ca. 61° 2θ, as a result of the low crystallinity of the samples.

The cell parameters *c* and *a* of the rhombohedral structure were calculated from the position of the (003) and (110) diffraction lines, respectively, assuming a 3R stacking of the layers ($c = 3d_{003}$ and $a = 2d_{110}$). The *a* cell parameter is equivalent to the mean distance between adjacent cations in the cationic brucite-type layers, and is correlated with the average value of radii of the metal cations in the layer.[39] Generally, this parameter decreases with increasing values of x in the formula $[M^{2+}_{1-x}M^{3+}_x(OH)_2](CO_3^{2-})_{x/2} \cdot yH_2O$, that is, with the degree of substitution, due to the smaller radius of Al^{3+} than that of Ni^{2+}. In other words, the *a* cell parameter decreases with the Ni/Al ratio. This is confirmed from sample Ni_3Al-P to Ni_1Al-P, which is consistent with the increase in aluminum content (Table 1).
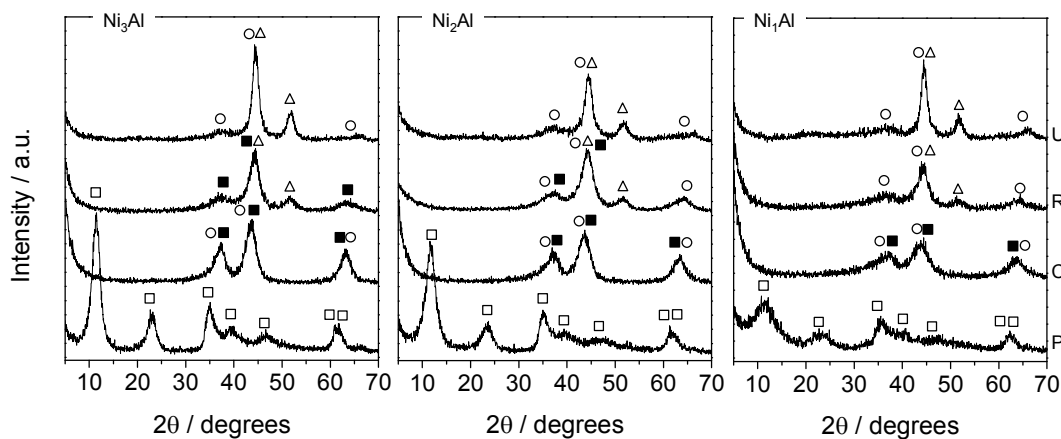
Fig. 1 XRD patterns of the as-synthesized takovites (P) and the products of calcination at 450°C (C), reduction (R) and after use in the reaction (U). Crystalline phases: (□) takovite, (■) Ni(Al)O$_x$, (○) NiAl$_2$O$_4$, and (△) Ni^0.

Similarly, the *c* parameter also decreased as the layer thickness decreases, that is, with lower Ni/Al ratios.

Table 1 Characterization data of the as-synthesized takovites.

Sample	M^{2+}/ M^{3+a} / -	*c* / nm	*a* / nm	D$_{(003)}$ (D$_{(110)}$)^b/ nm	V$_p$ / cm^3 g^{-1}	S$_{BET}$ / m^2 g^{-1}
Ni$_3$Al	2.97	2.3129	3.0365	3.3 (10.6)	0.193	37.3
Ni$_2$Al	1.95	2.2559	3.0222	2.4 (14.1)	0.154	30.3
Ni$_1$Al	0.73	2.2502	2.9841	2.0 (5.0)	0.104	45.0

^{a} Molar metal ratio in solid by ICP-OES. ^{b} Average crystallite size estimated by Scherrer analysis applied to the (003) or (110) reflection, respectively.

Samples were mesoporous, with total pore volumes of 0.19, 0.15, and 0.10 cm^3 g^{-1}, and BET surface areas of ca. 38, 30, and 45 m^2 g^{-1}, for Ni$_3$Al-P, Ni$_2$Al-P, and Ni$_1$Al-P, respectively. Thermogravimetric analysis in air showed the typical two-step decomposition pattern of anionic clays, with a total weight loss of 35%, 33% and 35% for Ni$_3$Al-P, Ni$_2$Al-P, and Ni$_1$Al-P, respectively (Fig. 2). These values are in agreement with the theoretical weight losses of the pure takovites calculated based upon their chemical formulae, with the exception of the Ni$_1$Al-P sample, which exhibits a more pronounced lower total weight loss with respect to the theoretical value (42.7%). This difference may be due to the incomplete precipitation of the takovite phase, due to the formation of other phases with low crystallinity, not visible by XRD. Transition temperatures occur at ca. 135-175°C for the removal of interlayer water, and ca. 295-330°C, for dehydroxylation and decarbonation of the sheets, in agreement with previous works in the literature.[40] The second transition temperature is very similar for Ni$_3$Al-P and Ni$_2$Al-P, and is shifted to slightly lower values in Ni$_1$Al, indicating the higher stability of the former two samples.
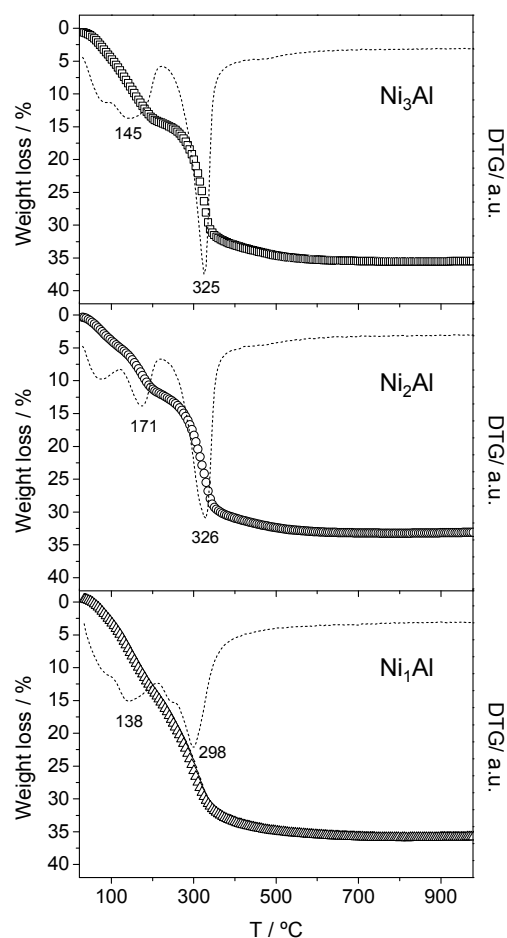

Fig. 2 Thermogravimetric analysis of the as-synthesized takovite samples in air and derivative of the weight loss.
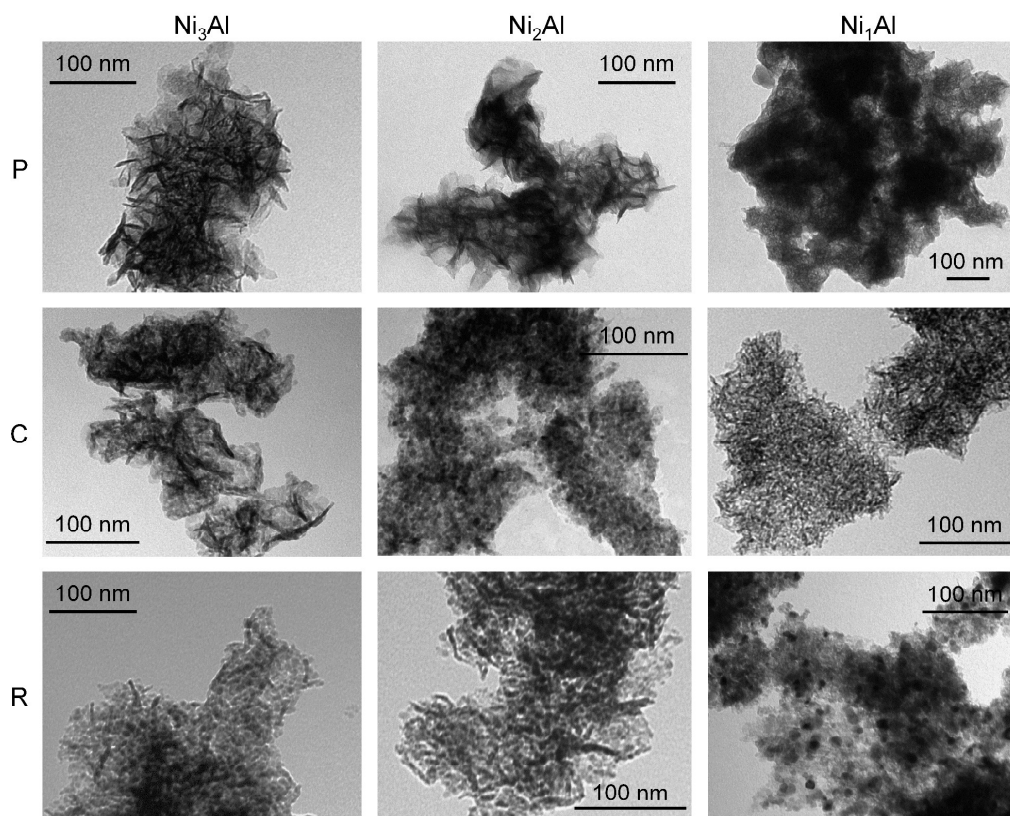
Fig. 3 TEM micrographs of the different samples.

Table 2. Characterization data of the calcined, reduced and used catalysts.

Sample code	Phase composition[a] / %			Crystallite size[b] / nm			S_{Ni}[c]/m^2 g^{-1}	D^c / %	V_p / cm^3 g^{-1}	S_{BET} / m^2 g^{-1}
	Ni(Al)O$_x$	NiAl$_2$O$_4$	Ni	Ni(Al)O$_x$	NiAl$_2$O$_4$	Ni				
Ni$_3$Al-C	78	21	-	2.96	1.4	-	-	-	0.404	162.9
Ni$_2$Al-C	66	34	-	2.3	0.6	-	-	-	0.394	187.1
Ni$_1$Al-C	53	46	-	1.7	0.6	-	-	-	0.319	168.7
Ni$_3$Al-R	66	-	33	1.3	-	3.4	11.66	2.74	0.333	124.8
Ni$_2$Al-R	50	25	25	1.53	1.6	3.1	10.14	2.61	0.370	136.2
Ni$_1$Al-R	-	87	13	-	0.6	3.0	5.13	1.90	0.371	167.8
Ni$_3$Al-U[d]	-	56	44	-	0.95	4.0	-	-	0.321	103.5
Ni$_2$Al-U[d]	-	73	27	-	0.85	3.2	-	-	0.414	136.8
Ni$_1$Al-U[d]	-	64	36	-	1.2	4.4	-	-	0.244	95.2
Ni$_2$Al-U[e]	-	65	34	-	0.9	3.1	-	-	0.383	121.3

[a] Crystalline phase composition determined by Rietveld refinement. [b] Average crystallite size obtained by refinement of the whole profile. The weighted residual error was in the range 0.5-5% for both crystallite size and phase composition. [c] Determined by H$_2$-chemisorption. [d] Used catalysts in experiments conducted using a pressure of 10.0 bar(g). [e] Used catalyst in an experiment conducted using a pressure of 1.0 bar(g).

The morphology of the three samples was investigated by transmission electron microscopy (TEM), as shown in Fig. 3. All samples exhibited the fibrous features or platelet-like morphology typical of hydrotalcites.[39] However, well-defined plate-like particles were clearly discerned in the Ni$_3$Al-P sample, while tightly aggregated particles were present in Ni$_1$Al-P. In good correspondence with XRD, the platelet dimensions in Ni$_1$Al-P were considerably smaller than those in Ni$_3$Al-P.

Thermal decomposition

As shown in Fig. 1, the solids calcined at 450°C showed characteristic reflections of the NiO-bunsenite structure (47-1049 ICDD pattern). NiO reflections are shifted to higher 2θ values than those corresponding to pure NiO, due to Al^{3+} substitution in the nickel oxide lattice and the formation of a solid solution, hereafter labeled as Ni(Al)O. Alzamora et al.[22] first, and Titulaer et al.[41] later claimed that takovite decomposition occurs through formation of a disordered spinel intermediate phase, composed of NiO containing some Al ions, and a nickel containing alumina phase, which is a very poorly ordered Ni deficient spinel $Ni_{1.8}Al_{2+2\delta/3}O_4$. Although the presence of a spinel phase was not clear by simple inspection of XRD patterns, a quantitative analysis of phases by Rietveld refinement enabled to detect spinel phases in practically all samples (Table 2). The presence of the above mentioned solid solution was confirmed by determination of the *a* cell parameter in the three samples and compared to that of pure NiO (0.4177 nm); 0.4150(4) nm for Ni3Al-C, 0.4143(3) nm for Ni2Al-C, and 0.4120(6) nm for Ni1Al-C. Although higher temperatures are necessary for pure takovite samples to segregate into $NiAl_2O_4$ spinel,[42] a certain amount of this phase was detected in the samples. In fact, the percentage of spinel increases with the increase in aluminum content, that is, with lower Ni/Al ratios, and the opposite applied to the Ni(Al)O phase. This is somehow expected attending to the lower amount of nickel required for spinel formation; in other words, the excess of Al^{3+} in takovites with Ni/Al = 1, is not completely replacing Ni^{2+} in the nickel oxide lattice, thus leading to a higher predilection for spinel segregation. Despite the largest amount of spinel in Ni1Al-C, the *a* cell parameter is far below that of pure NiO; the NiO reflection is progressively shifted to higher 2θ values upon decreasing the Ni/Al ratio. This indicates that aluminum is incorporated in the bunsenite structure in all cases, but in Ni1Al-C, the formation of the spinel is favored due to the required stoichiometric ratio, and the rest of aluminum is well integrated in the Ni(Al)O solid solution. Upon increasing the nickel content, the amount of spinel decreases and the a cell parameter increases, approaching the value of pure NiO.

The Ni(Al)O average crystallite size was estimated at 2.96 nm in Ni3Al-C (Table 2). The crystallite size also decreases with the increase in aluminum content. Concerning the spinel phase, small average crystallites are formed, which are certainly in the limit for accurate crystallite size determinations. Reflections related to $NiAl_2O_4$ and Ni(Al)O are completely superimposed in the diffractogram; in those cases where the size was smaller than the limit imposed by the technique itself (here 0.6 nm), the crystallite size was difficult to be calculated, as it could not be easily discerned from the background.

Thermal decomposition of the takovite-derived precursors at 450°C led to the transformation from fibrous to rounded nanoparticles, with a size distribution in the range 4–10 nm in the derived Ni(Al)O mixed oxides. Some whisker-like particles were still present in the Ni3Al-C sample, while the nodular particles intermingled between platelets were clearly visible in

Ni2Al-C and Ni1Al-C (Fig. 3). Calcined samples were mesoporous, and their porosity was greatly increased from that of the starting takovite precursors, reaching a total pore volume in the range 0.32-0.40 $cm^3 g^{-1}$, and BET surface areas of 160-190 $m^2 g^{-1}$.

Reduction

The temperature programmed reduction profile for the three samples is shown in Fig. 4. The reduction of nickel takes place in the broad range of temperatures associated with the reduction of takovite-derived oxide samples, that is, 400-825°C.[43-46] The reduction of pure NiO usually exhibits a single reduction peak at 337-397°C.[47,48] As previously reported, the presence of aluminum on the mixed oxide causes a shift to higher reduction temperatures.[22,44,46] This is clearly observed in the three samples, in which the increasing amount of aluminum moves the peak maxima to a similar temperature of ca. 647 °C. As expected, the area of H_2 consumption follows the order Ni3Al-C>Ni2Al-C>Ni1Al-C. The Ni1Al-C sample shows a symmetrical peak of hydrogen consumption centered at 643°C, with a small shoulder at 479°C. With the increase in Ni content, a shoulder of noticeable intensity appears at 737°C. As described by the model of Puxley et al.[43] for nickel/alumina catalysts, the observed profile corresponds to the co-reduction of various structures containing nickel, i.e. the disordered spinel intermediate phase, composed of NiO containing some Al ions, and the nickel containing alumina phase (Ni deficient spinel).
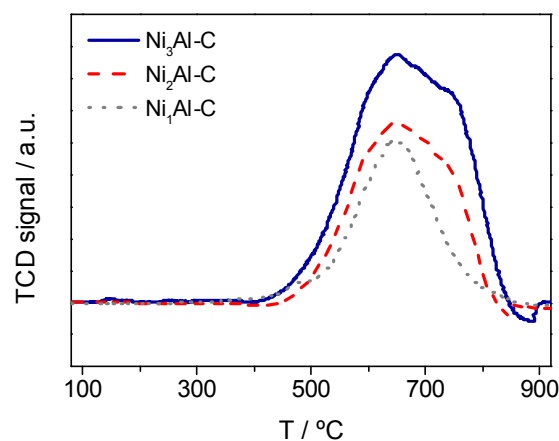

Fig. 4 H_2-TPR profiles of the calcined takovites.

Reduction of the calcined samples before reaction (samples were reduced under similar conditions than before activity tests for characterization purposes) led to the decrease of the original Ni(Al)O reflections (superimposed to the spinel reflections), concomitantly to the appearance of two reflections at 2θ 44° and 52° (4-850 ICDD pattern), associated with metallic nickel (Fig. 1). Based on the quantitative analysis of the phases present in the reduced samples by Rietveld refinement, the reduction process resulted to be incomplete in all cases. Since some oxidation might be expected from contact in air, this analysis gives a percentage of Ni^0 that might

be slightly lower than if passivation was performed. However, the fact that no NiO was encountered in the Ni$_1$Al-R after reduction and subsequent XRD analysis indicates that the oxidation of reduced catalysts was minimized. As shown in Table 2, the percentage of metallic nickel is relatively low after the reduction treatment (33% for Ni$_3$Al-R, 25% for Ni$_2$Al-R, and 13% in Ni$_1$Al-R). This indicates that the catalysts, despite similar treatments, experienced partial reduction under the selected conditions: the amount of Ni^0 after reduction strongly depends on the amount of aluminum, that is, on the propensity for spinel formation, following the order Ni$_3$Al-R<Ni$_2$Al-R<Ni$_1$Al-R. That is, as the Ni/Al ratio decreases, the formation of spinel is favored, and therefore, the reduction process is slowed down. This is expected considering the reduction profiles for each of the calcined samples (Fig. 4). Besides, in parallel to Ni(Al)O disappearance, the percentage of spinel increased with respect to the calcined samples, indicating that part of the solid solution is reduced into metallic nickel and the rest is transformed into the most stable phase, NiAl$_2$O$_4$. The Ni^0 average crystallite size, estimated by the Rietveld refinement method, was in the range of 3-3.4 nm, values slightly smaller than previous reported crystallite size in takovite sample with Ni/Al = 3.[31]

Transmission electron microscopy and N$_2$ adsorption were carried out over the reduced samples to check the variations in morphology and texture with respect to the oxide precursor. All three reduced samples exhibited the nodular morphology already observed in the Ni(Al)O mixed oxides, with sizes in the range of 6-17 nm. As shown in Table 2, the reduction treatment decreased the BET surface area of the Ni$_3$Al-R and Ni$_2$Al-R samples, while the Ni$_1$Al-R sample was maintained in the same order.

Hydrogen chemisorption measurements were conducted in order to determine the nickel surface area and nickel dispersion in the reduced samples. It is important to note that chemisorption experiments were directly analyzed after reduction, and the amount of metallic nickel in the Ni$_x$Al-R samples might vary from the results quantified from XRD (attained after contact in air). Table 2 shows that the Ni$_1$Al-C sample exhibits the lowest nickel surface area (with the lowest monolayer uptake, according to the lower amount of nickel in this sample). In fact, both metal surface areas and metal dispersion increase with the Ni/Al ratio.

Catalyst screening

The three takovite-based mixed oxides were tested in the reaction. Fig. 5 displays a typical temperature profile of a complete screening experiment and the variation in conversion and product selectivity with reaction temperature (catalyst Ni$_1$Al-C, 10 bar(g), WHSV of 0.6 mol$_{CO2}$/(g$_{cat}$ h) and a

H$_2$/CO$_2$ molar ratio of 4). After reducing the catalyst in situ at 500°C for 3 h under 10% H$_2$ in nitrogen, CO$_2$ and H$_2$ were started to feed, and the catalyst was maintained at 400°C for 5 h. Afterwards, the reaction temperature was decreased to 225°C in steps of 25°C, being maintained at each value for 5 h. Temperature was subsequently raised again to 400°C following the same temperature steps, to check for deactivation or any change in products selectivity. CO$_2$ conversion was maintained practically at 95% in the range 400-325°C, with methane being the major product (ca. 99% selectivity) besides water, and very small amount of carbon monoxide and traces of ethane. As expected, the decrease in temperature from 325°C to lower temperatures produced a pronounced reduction in CO$_2$ conversion, reaching values of ca. 60% at 300°C, 24% at 275°C, or just ca. 3% at 225°C. This catalyst was very stable at each of the different temperatures. After raising the temperature back to 400°C, the results in both CO$_2$ conversion and product selectivity were nearly identical to those obtained at the beginning of the experiment.

The results obtained under this experimental procedure for all the Ni$_x$Al-C catalysts, both in terms of conversion and selectivity at each temperature were averaged using those points corresponding to stable operation intervals (i.e. 5 h in all cases), and the confidence intervals for the average values calculated at the 99% probability level. Experimental conditions were maintained (10 bar (g), WHSV of 0.6 mol$_{CO2}$/(g$_{cat}$ h) and a H$_2$/CO$_2$ molar ratio of 4), and the results of CO$_2$ conversion and product selectivity were plotted with respect to reaction temperature (Fig. 6). Previous results with a high-loaded nickel based catalyst, used at the same experimental conditions, were also included for comparison.[30] At temperature above 325°C, carbon dioxide conversion and the selectivity to methane and carbon monoxide were very close to their corresponding equilibrium values irrespective of the catalyst Ni/Al ratio. The Ni$_5$Al catalyst from our previous work reached the equilibrium conversion at 350°C. Below this temperature, CO$_2$ conversion did not achieve the equilibrium under the conditions employed, thus leading to a slightly decreased CH$_4$ selectivity and an increased CO and ethane selectivity with respect to the equilibrium values. This effect was remarkable in the catalyst with lower Ni/Al ratio, i.e. Ni$_1$Al-C, whose carbon monoxide selectivity was nearly 5% at 300°C and ca. 9% at 250°C. The Ni$_2$Al-C and Ni$_3$Al-C catalysts behaved similarly in terms of CO$_2$ conversion and product selectivity, although the former exhibited a slightly higher conversion in the range 250-300°C and lower CO and ethane selectivity in the range 300-350°C. These results indicated that the Ni$_2$Al-C catalyst, with a moderate average Ni surface area and dispersion compared to Ni$_1$Al-C (Table 2), was the most active and selective in the temperature range investigated.
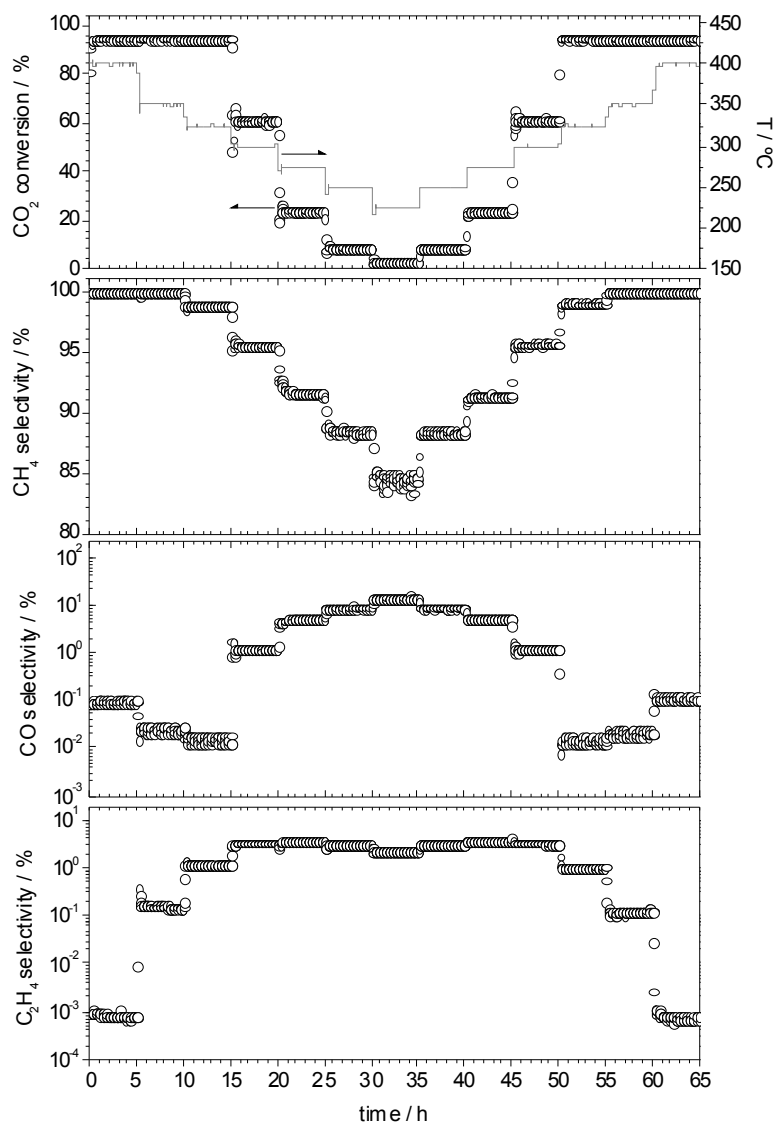
Fig. 5 Temperature profile, carbon dioxide conversion and product selectivity towards methane, carbon monoxide and ethane during a typical catalyst screening experiment (Ni1Al-C catalyst, H2/CO2 and N2/CO2 molar ratios of 4 and 1, WHSV of 0.6 molCO2/(gcat h) and 10 bar(g).

The Ni_2Al-C catalyst was subsequently tested at 1 bar(g), maintaining a WHSV of 0.8 $mol_{CO2}/(g_{cat}$ h) and a H_2/CO_2 molar ratio of 4. In fact, the carbon dioxide methanation has been extensively conducted at atmospheric pressure,[27] and it was interesting to observe the behavior of the takovite-derived catalyst at low pressure. Fig. 7 compares CO_2 conversion and product selectivity, showing that both equilibrium conversion and selectivity were achieved at 350°C, irrespective of the pressure used. Below this temperature, CO and ethane selectivity were significantly higher than equilibrium values, while that of methane was slightly lower than equilibrium. The effect of increasing pressure from 1 to 10 bar led to slightly higher conversions, higher CH_4 selectivity and lower CO and ethane selectivity when working below equilibrium conditions.

This suggests that the higher pressure induced a slightly higher concentration of adsorbed hydrogen atoms on the catalyst surface, thus promoting a relatively higher reaction rate. Our previous work using a catalyst prepared by coprecipitation and high Ni loading indicated that the preparation method can induce the formation of well dispersed Ni^0 crystallites (6 nm) dispersed over a NiO-alumina, which are active and very selective for CO_2 methanation.[30] Herein, following the same route, takovite-derived mixed oxide catalysts have exhibited high catalytic performance, induced by their intrinsic features. Despite the high nickel loading compared to conventional Ni/Al_2O_3 catalysts prepared by impregnation, small Ni crystallites are obtained (in the order 1.9-3 nm), which remain dispersed in a high surface area Ni(Al)O matrix.
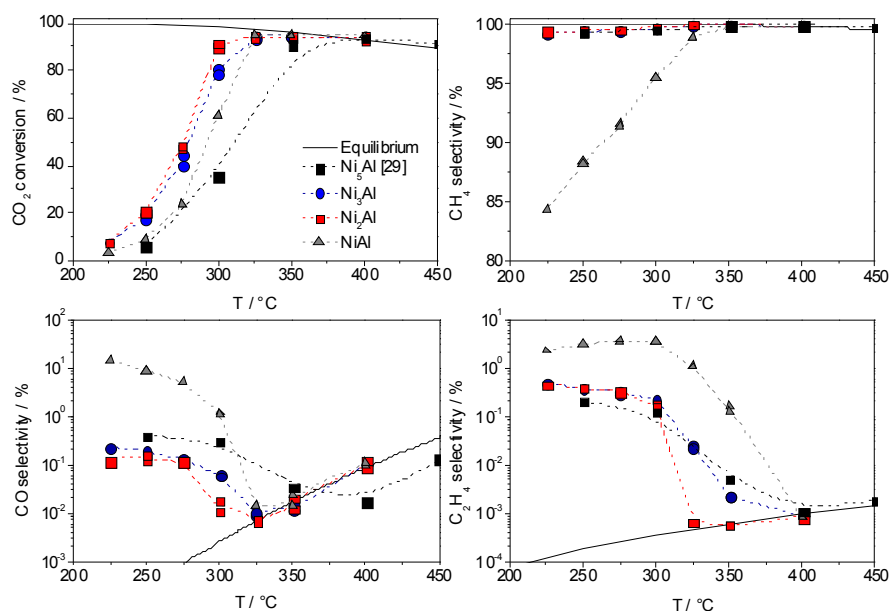
Fig. 6 Influence of catalyst composition on the average carbon dioxide conversion and product selectivity at 225 - 400°C, and comparison with chemical equilibrium. All experiments performed at a WHSV of 0.6 mol$_{CO2}$/(g$_{cat}$ h), 10.0 bar(g), and H$_2$/CO$_2$ and N$_2$/CO$_2$ molar ratios of 4 and 1, respectively.
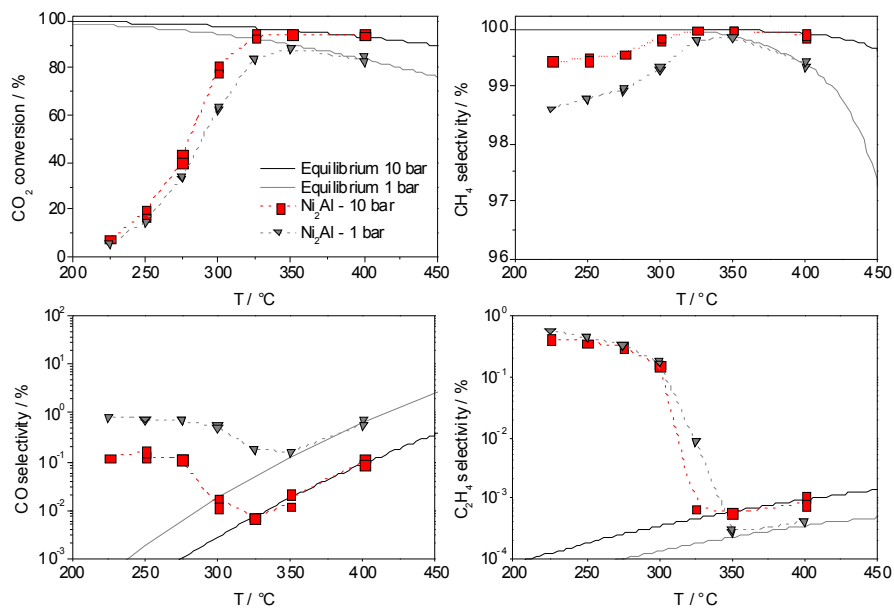

Fig. 7 Influence of reaction pressure on the average carbon dioxide conversion and product selectivity at 225 - 400°C using the Ni$_2$Al-C catalyst, and comparison with chemical equilibrium. All experiments performed at a WHSV of 0.6 mol$_{CO2}$/(g$_{cat}$ h), and H$_2$/CO$_2$ and N$_2$/CO$_2$ molar ratios of 4 and 1, respectively.

Lifetime testing

Taking into account the above results, the Ni$_2$Al-C catalyst was also selected to perform lifetime tests to observe its stability upon time on stream. Tests were conducted at atmospheric pressure, WHSV of 0.8 mol$_{CO2}$/(g$_{cat}$ h) and a H$_2$/CO$_2$ molar ratio of 4. The space velocity was increased with respect to previous experiments in order to subject the catalyst to a lower contact time with the reactants, and check for differences in both

conversion and selectivity. Besides, this space velocity is practically one order of magnitude larger than the space velocities typically used on catalyst development studies.[30] Fig. 8 displays the CO_2 conversion and product selectivity in two long experiments of more than 500 h at two different temperatures, 275 or 350°C. The average CO_2 conversion and CH_4 selectivity in the first hour was 74% and 99.2% at 350°C, respectively, with 0.7% of CO and trace amounts of ethane. The catalyst experienced a slight decrease in activity, which only reduced the CO_2 conversion to an average value of 72.8% in the last 50 h of reaction. In parallel, the CH_4 selectivity was 98.9%, with no change in ethane selectivity, and ca. 1% of CO. As expected, the reaction at 275°C led to lower CO_2 conversion (66%) and CH_4 selectivity (98.7%), values that were practically maintained until the end of the experiment (495 h). At this temperature, both the CO and ethane selectivity were constant along the experiment, but ethane exhibited a higher content than experiments at higher temperature.
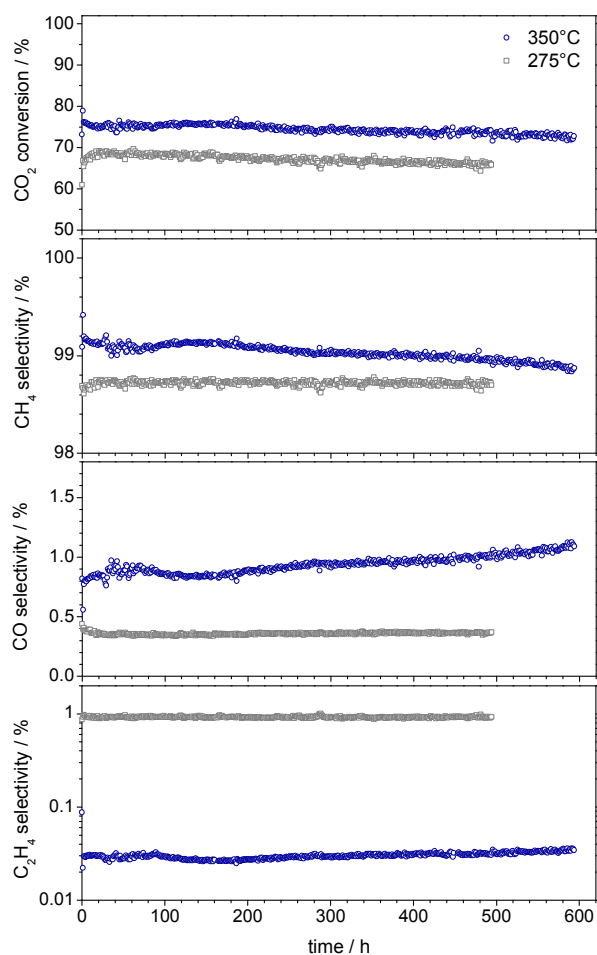

Fig. 8 Lifetime catalyst activity test (500-600 h). Carbon dioxide conversion and product selectivity using the Ni_2Al-C catalyst at 350 and 275°C, atmospheric pressure, a WHSV of 0.8 $mol_{CO2}/(g_{cat} h)$, and H_2/CO_2 and N_2/CO_2 molar ratios of 4 and 1, respectively.

Our previous work, dealing with a Ni-Al catalyst prepared by coprecipitation with a high Ni loading (ca. 70 wt.%, Ni/Al = 5) demonstrated the high catalytic performance of the resulting Ni crystallites over a partially reduced Ni(Al)O matrix.[30] In that case, using drastic experimental conditions (400 °C, 10 bar(g), WHSV of 2.0 $mol_{CO2}/(g_{cat} h)$, and H_2/CO_2 = 4), the CO_2 conversion was around 83% with >99% CH_4 selectivity after a 490 lifetime test. Herein, the properties of the resulting small Ni crystallites (ca. 3-4 nm) dispersed over a Ni(Al)O-NiAl$_2O_4$ matrix have induced high catalytic performance in CO_2 methanation, being particularly stable for long time on stream reactions. In agreement with He et al.,[31] smaller nickel crystallites are beneficial for CO_2 methanation.

Infrared studies

Operando FTIR studies were performed to check for adsorbed species during reaction. Fig. 9 shows the infrared spectra of CO_2 adsorption (top) and CO_2 methanation (bottom) over the most active and selective Ni$_2$Al-C catalyst in the temperature range 150-400°C. As previously reported in the literature, bands in the region 1700-1000 cm^{-1} are related to carbonate-like species, in this case, adsorbed in the freshly reduced Ni(Al)O/NiAl$_2O_4$ sample. Typically, CO_2 reacts with surface oxygen to form hydrogen carbonates, bidentate and monodentate carbonates, which exhibit different stabilities.[21] The spectra for CO_2 adsorption at 150°C shows bands at 1582, a shoulder at 1509, a small shoulder at 1395, 1340, 1195, 1070, and bands at >3500 cm^{-1}. In the range of 2240-1850 no bands related to CO are observed. All these bands experience a progressive increase in intensity upon increasing the reaction temperature, with the exception of the bands >3000 cm^{-1}, which give indication of the strong stability of these species. According to the literature, the band at 1582 belong to bidentate carbonates, while the other observed bands seem to belong to monodentate carbonates formed over the surface. In contrast to similar infrared studies over Ni/γ-Al$_2O_3$[21] or Ni/Ce$_{0.5}$Zr$_{0.5}$O$_2$[21] where bidentates and monodentate carbonates decrease their intensity upon increasing temperature, herein, these species are much more stable in the same temperature range.

The incorporation of H_2 during methanation experiments does not affect the bands previously detected for CO_2 adsorption studies. Monodentate and bidentate species are clearly visible in all the temperature range investigated, although a decreased intensity of the bands was noticed above 300°C. At 250°C, new absorption bands appear at 1747 and a shoulder at 1566 cm^{-1}, which are likely related to OCO stretching vibration of formate species.[21] The intensity of formate species increases until 300°C, is maintained at 350°C, and then decreases drastically. Bidentate carbonates at ca 1580 cm^{-1} start to decrease their intensity at 300°C, and are practically vanished at 400°C. According to Pan et al.,[21] the formation of formate is due to hydrogenation of monodentate carbonates, while Westermann et al.[49] attributed these species to a surface reaction between dissociated and physisorbed or adsorbed perturbed CO_2 molecules. Also, two characteristic methane bands at 3015 and 1303 cm^{-1} are visible at 300°C. Further increase of the reaction temperature to 400°C resulted in increased methane intensity, with a reduction of formate

species at 1756 cm^{-1}, and the presence of CO (ca. 2150 cm^{-1}). No Ni^0-carbonyls are clearly detected in the region 2080-1880 cm^{-1}, as observed in Ni/silica catalysts.[50]

Two mechanisms for CO$_2$ methanation have been proposed in the literature.[20,50,51] The first one suggests the formation of formate species as main intermediate, which are adsorbed on the support.
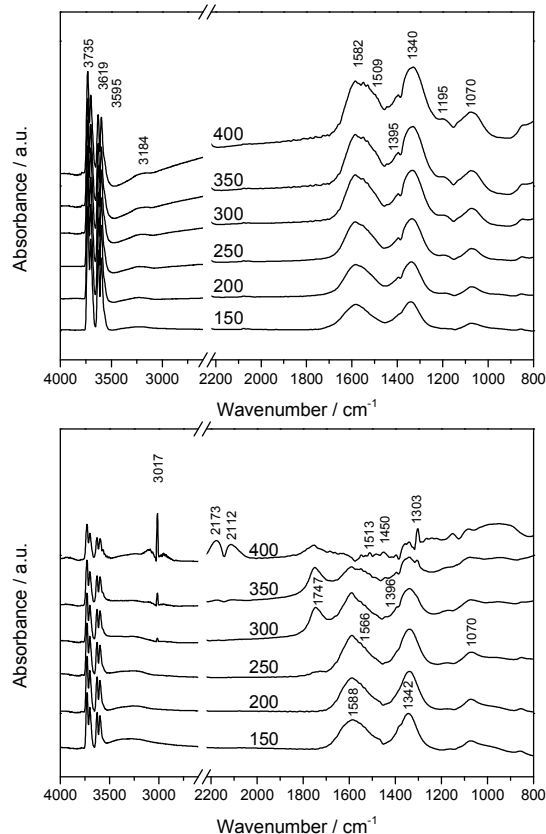

Fig. 9 FTIR spectra of CO$_2$ adsorption (top) and CO$_2$ methanation (bottom) over Ni$_2$Al-C catalyst at different temperatures in the range 150-400°C.

These species are decomposed to CO, which is further transformed to methane with hydrogen. The second mechanism relies in the dissociation of CO$_2$ in CO and O adsorbed species, or the transformation of CO$_2$ to CO + H$_2$O via reverse water gas shift; CO is claimed as the intermediate that will further react with hydrogen to form methane (in this case, without formation of formate species). Despite the number of studies dealing with this reaction, and similarly to the CO methanation reaction, there is still no consensus on the mechanism. From these two plausible mechanisms, there are also two possible rate-determining steps; the formation of the CHxO intermediate and its hydrogenation, or the formation of surface carbon in CO dissociation and its reaction with hydrogen.

Considering the main species formed over Ni$_2$Al-C catalyst, the main reaction pathway seems to occur through the adsorption of CO$_2$ in sites of mild basicity to form carbonates (monodentates and bidentates, no hydrogen carbonates seem to be present). These carbonates are further reduced by H

atoms, formed by dissociation of H$_2$ on the surface of Ni^0 to generate formate species, which are converted to methoxy species, to finally release methane. Although the second mechanism of CO$_2$ dissociation or reverse water gas shift cannot be excluded, the presence of bands associated to formate species make the first mechanism to gain ground for this type of Ni/NiAl$_2$O$_4$ catalysts.

Characterization of the spent catalysts

The different catalysts after reaction were characterized by XRD and N$_2$ adsorption. The XRD patterns of each used catalyst are shown in Fig. 1. In all cases, metallic nickel reflections with higher intensity compared to the fresh Ni$_x$Al-R catalysts are observed, as confirmed by Rietveld refinement in Table 2. No Ni(Al)O reflections were discerned from these data in the used samples, confirming the in situ reduction of this phase and the partial transformation into spinel. These results contrast with our previous study over a high-loaded Ni$_5$Al catalyst, exhibiting a 100% Ni^0, derived from reduction of the Ni(Al) mixed oxide phase. The high amount of nickel in that sample with respect to aluminum, avoided the formation of spinel phase at the same reaction conditions.[30] The average Ni^0 crystallite size of all samples amounted 4, 3.2, and 4.4 nm for Ni$_3$Al-U, Ni$_2$Al-U, and Ni$_1$Al-U, respectively. These results clearly indicate that practically no sintering occur upon reaction. Concerning the spinel phase, the average crystallite size increases with respect to the minimum value detected in the reduced samples (not clearly discerned from the background), confirming the presence of this phase in all samples. Besides, the NiAl$_2$O$_4$ crystallite size grew up in the sample with higher aluminum content (Ni$_1$Al-U), in agreement with the higher propensity of this ratio for spinel formation.

N$_2$ adsorption revealed a slightly lower surface area in the used catalysts probably due to coke residues (not visible by XRD), and this decay was more pronounced in the Ni$_1$Al-U sample (Table 2). However, no carbonaceous deposits were observed over the used catalysts by TEM, even after the reaction test of 490 h (Fig. 10).
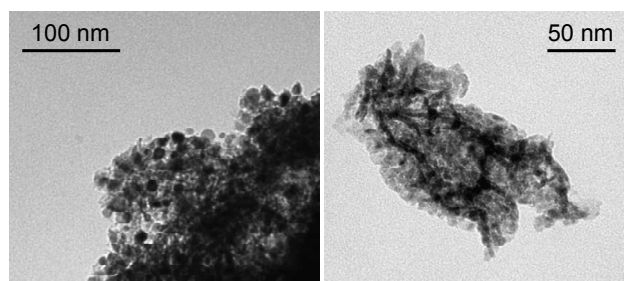

Fig. 10 TEM micrographs of the Ni$_2$Al-U sample.

Conclusions

Ni-Al mixed oxides with Ni/Al molar ratios from 1 to 3 were prepared from takovite precursors and evaluated in their (partially)reduced form in CO$_2$ methanation. Activation treatments based on calcination followed by reduction at

selected conditions led to a decreasing amount of metallic nickel, and increasing amount of spinel upon decreasing the Ni/Al ratio. This is due to the higher propensity of takovites with lower Ni/Al ratio to form a spinel phase, which in turn, was more stable towards nickel reduction. The characterization of used catalysts indicated the *in situ* reduction upon time on stream, although all catalysts were only partially reduced as a result of the presence of small $NiAl_2O_4$ crystallites. The results indicated that the Ni_2Al-C catalyst, was the most active and selective in the temperature range investigated. The properties of the resulting small Ni crystallites (ca. 3-4 nm) dispersed over the $NiAl_2O_4$ matrix have induced high catalytic performance in CO_2 methanation, being particularly stable for long time on stream reactions. Neither sintering nor carbon deposition occurs upon reaction in any catalyst, suggesting that well-dispersed Ni^0 crystallites over the spinel phase are essential to attain active and stable catalysts. The information concluded from infrared studies indicates that the mechanism of CO_2 methanation over $Ni/NiAl_2O_4$ catalysts goes through the formation of carbonates, further reduced to formate species, which are finally converted to methoxy species and subsequent CH_4 molecules.

Acknowledgements

Notes and references

1 International Energy Outlook 2014, http://www.eia.gov/forecasts/ieo/pdf/0484(2014).pdf, (accessed 01/03/2015).
2 G. Centi and S. Perathoner, *Catal. Today*, 2009, **148**, 191-205.
3 J. Kopyscinski, T. J. Schildhauer and S. M. A. Biollaz, *Fuel*, 2010, **89**, 1763–1783.
4 P. Sabatier and J. B. Senderens, *C. R. Acad. Sci.*, 1902, **134**, 689-691.
5 J. E. Gallagher and C. A. Euker, *Int. J. Energy Res.*, 1980, **4**, 137.147.
6 M. Gassner and F. Maréchal, *Biomass Bioenergy*, 2009, **33**, 1587-1604.
7 S. K. Hoekman, A. Broch, C. Robbins and R. Purcell, *Int. J. Greenhouse Gas Control*, 2010, **4**, 44-50.
8 A. Molino and G. Braccio, *Fuel*, 2015, **139**, 425-429.
9 M. A. A. Aziz, A. A. Jalil, S. Triwahyono and A. Ahmad, *Catal. Sci. Technol.*, 2015, **17**, 2647-2663.

10 G. A. Mills and F. W. Steffgen, *Catal. Rev. - Sci. Eng.*, 1974, **8**.
11 J. L. Falconer and A. E. Zağli, *J. Catal.*, 1980, **62**, 280-285.
12 G. D. Weatherbee and C. H. Bartholomew, *J. Catal.*, 1981, **68**, 67-76.
13 G. D. Weatherbee and C. H. Bartholomew, *J. Catal.*, 1982, **77**, 460-472.
14 A. E. Aksoylu and Z. I. Onsan, *Appl. Catal. A*, 1997, **164**, 1-11.
15 F.-W. Chang, M.-S. Kuo, M.-T. Tsay and M.-C. Hsieh, *Appl. Catal. A*, 2003, **247**, 309-320.
16 D. C. D. da Silva, S. Letichevsky, L. E. P. Borges and L. G. Appel, *Int. J. Hydrogen Energy*, 2012, **37**, 8923-8928.
17 S. Tada, T. Shimizu, H. Kameyama, T. Haneda and R. Kikuchi, *Int. J. Hydrogen Energy*, 2012, **37**, 5527-5531.
18 F. W. Chang, M. T. Tsay and S. P. Liang, *Appl. Catal. A*, 2001, **209**, 217-227.
19 G. A. Du, S. Lim, Y. H. Yang, C. Wang, L. Pfefferle and G. L. Haller, *J. Catal.*, 2007, **249**, 370-379.
20 W. Wang, S. Wang, X. Ma and J. Gong, *Chem. Soc. Rev.*, 2011, **40**, 3703-3727.
21 Q. Pan, J. Peng, T. Sun, D. Gao, S. Wang and S. Wang, *Fuel Proces. Technol.*, 2014, **123**, 166-171.
22 L. E. Alzamora, J. R. H. Ross, E. C. Kruissink and L. L. van Reijen, *J. Chem. Soc., Faraday Trans. 1*, 1981, **77**, 665-681
23 J. R. H. Ross, in *Catalysis*, eds. G. C. Bond, G. Webb and J. R. H. Ross, RSC, London, 1985, vol. 7, pp. 1-45.
24 A. E. Aksoylu, A. N. Akin, Z. I. Önsan and D. L. Trimm, *Appl. Catal. A*, 1996, **145**, 185-193.
25 A. Zhao, W. Ying, H. Zhang, H. Ma and D. Fang, *Catal. Commun.*, 2012, **17**, 34-38.
26 S. Rahmani, M. Rezaei and F. Meshkani, *J. Ind. Eng. Chem.*, 2014, **20**, 1346-1352.
27 G. Garbarino, P. Riani, L. Magistri and G. Busca, *Int. J. Hydrogen Energy*, 2014, **39**, 11557-11565.
28 P. Riani, G. Garbarino, M. A. Lucchini, F. Canepa and G. Busca, *J. Mol. Catal. A*, 2014, **383-384**, 10-16.
29 S. Hwang, U. G. Hong, J. Lee, J. G. Seo, J. H. Baik, D. J. Koh, H. Lim and I. K. Song, *J. Ind. Eng. Chem.*, 2013, **41**, 2016-2021.
30 S. Abelló, C. Berrueco and D. Montané, *Fuel*, 2013, **113**, 598-609.
31 L. He, Q. Lin, Y. Liu and Y. Huang, *J. Energy Chem.*, 2014, **23**, 587-592.
32 M. Gabrovska, R. Edreva-Kardjieva, D. Cris, P. Tzvetkov, M. Shopska and I. Shtereva, *Reac. Kinet. Mech. Cat.*, 2012, **105**, 79-99.
33 H. M. Rietveld, *J. Appl. Cryst.*, 1969, **2**, 65-71.
34 R. Hill and C. Howard, *J. Appl. Crystallogr.*, 1987, **20**, 467-474.
35 TOPAS, *General Profile and Structure Analysis Software for Powder Diffraction Data, V4.2*, Karlsruhe, Germany, Bruker AXS GmbH.
36 D. Balzar, ed., *Voigt-function model in diffraction line-broadening analysis.*, Oxford University Press, New York, 1999.

37 A. Stokes and A. Wilson, *Math. Proc. Cambridge Philos. Soc.*, 1942, **38**, 313-322.

38 S. J. Mills, P. S. Whitfield, A. R. Kampf, S. A. Wilson, G. M. Dipple, M. Raudsepp and G. Favreau, *J. Geosci.*, 2012, **57**, 273-279.

39 F. Cavani, F. Trifirò and A. Vaccari, *Catal. Today*, 1991, **11**, 173-301.

40 M. Jitianu, D. C. Gunness, D. E. Aboagye, M. Zaharescu and A. Jitianu, *Mater. Res. Bull.*, 2013, **48**, 1864-1873.

41 M. K. Titulaer, J. B. H. Jansen and J. W. Geus, *Clays Clay Miner.*, 1994, **42**, 249-258.

42 O. Clause, B. Rebours, E. Merlen, F. Trifiró and A. Vaccari, *J. Catal.*, 1992, **133**, 231-246.

43 D. C. Puxley, I. J. Kitchener, C. Komodromos and N. D. Parkyns, in *Preparation of Catalysts III, Stud. Surf. Sci. Catal.*, eds. G. Poncelet, P. Grange and P. A. Jacobs, Elsevier Science, 1983, vol. 16, pp. 237-271.

44 O. Clause, M. G. Coelho, M. Gazzano, D. Matteuzzi, F. Trifirò and A. Vaccari, *Appl. Clay Sci.*, 1993, **8**, 169-186.

45 V. Mas, G. Baronetti, N. Amadeo and M. Laborde, *Chem. Eng. J.*, 2008, **138**, 602-667.

46 S. Abelló, D. Verboekend, B. Bridier and J. Pérez-Ramírez, *J. Catal.*, 2008, **259**, 85-95.

47 K. V. R. Chary, P. V. R. Rao and V. Vishwanathan, *Catal. Commun.*, 2006, **7**, 974-978

48 M. Li, X. Wang, S. Li, S. Wang and X. Ma, *Int. J. Hydrogen Energy*, 2010, **35**, 6699-6708.

49 A. Westermann, B. Azambre, M. C. Bacariza, I. Grac, M. F. Ribeiro, J. M. Lopes and C. Henriques, *Appl. Catal. B*, 2015, **174-175**, 120-125.

50 P. A. U. Aldana, F. Ocampo, K. Kobl, B. Louis, F. Thibault-Starzyk, M. Daturi, P. Bazin, S. Thomas and A. C. Roger, *Catal. Today*, 2013, **215**, 201-207.

51 A. Beuls, C. Swalus, M. Jacquemin, G. Heyen, A. Karelovic and P. Ruiz, *Appl. Catal. B*, 2012, **113-114**, 2-10.

Table of Contents entry
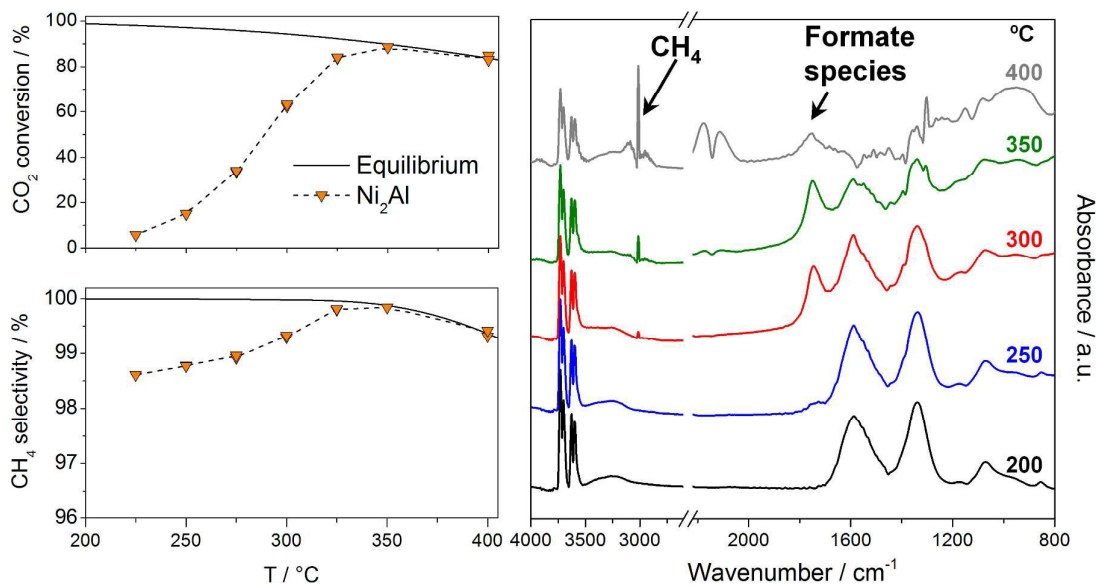
Small Ni^0 crystallites dispersed over $NiAl_2O_4$ matrix, attained from takovite-like precursors induced high catalytic performance in CO_2 methanation.